Geophysical Research Letters

RESEARCH LETTER
10.1029/2019GL085774

Compact Operational Tropospheric Water Vapor and Temperature Raman Lidar with Turbulence Resolution

D. Lange[1], A. Behrendt[1], and V. Wulfmeyer[1]

[1]Institute of Physics and Meteorology, University of Hohenheim, Stuttgart, Germany

Key Points:
- Fulfills World Meteorological Organization breakthrough requirements for nowcasting/very short range forecasting in the lower troposphere
- Resolves strength of the inversion layer at the planetary boundary layer top and elevated lids above during daytime and nighttime
- Provides statistics on turbulent fluctuations in water vapor and temperature simultaneously in the lower troposphere

Correspondence to:
D. Lange,
diego.lange@uni-hohenheim.de

Citation:
Lange, D., Behrendt, A., & Wulfmeyer, V. (2019). Compact operational tropospheric water vapor and temperature Raman lidar with turbulence resolution. *Geophysical Research Letters*, *46*, 14,844–14,853. https://doi.org/10.1029/2019GL085774

Received 13 SEP 2019
Accepted 21 NOV 2019
Accepted article online 13 DEC 2019
Published online 23 DEC 2019

Abstract We present the new Atmospheric Raman Temperature and Humidity Sounder (ARTHUS). We demonstrate that ARTHUS measurements resolve (1) the strength of the inversion layer at the planetary boundary layer top, (2) elevated lids in the free troposphere during daytime and nighttime, and (3) turbulent fluctuations in water vapor and temperature, simultaneously, also during daytime. Very stable and reliable performance was demonstrably achieved during more than 2,500 hr of operations time experiencing a huge variety of weather conditions. ARTHUS provides temperature profiles with resolutions of 10–60 s and 7.5–100 m vertically in the lower free troposphere. During daytime, the statistical uncertainty of the water vapor mixing ratio is <2 % in the lower troposphere for resolutions of 5 min and 100 m. Temperature statistical uncertainty is <0.5 K even up to the middle troposphere. ARTHUS fulfills the stringent WMO breakthrough requirements on nowcasting and very short range forecasting.

Plain Language Summary The observation of atmospheric moisture and temperature profiles is essential for the understanding and prediction of earth system processes. These are fundamental components of the global and regional energy and water cycles; they determine the radiative transfer through the atmosphere and are critical for the cloud formation and precipitation. Also, it is expected that the assimilation of high-quality, lower tropospheric WV and T profiles will result in a considerable improvement of the skill of weather forecast models particularly with respect to extreme events. Here we present the Atmospheric Raman Temperature and Humidity Sounder, an exceptional tool for observations in the atmospheric boundary layer during daytime and nighttime with a very short latency. This performance serves very well the next generation of very fast rapid-update-cycle data assimilation systems for nowcasting and short-range weather forecasting. Ground-based stations and networks can be set up or extended for climate monitoring, verification of weather, climate and earth system models, and data assimilation for improving weather forecasts.

1. Introduction

The observation of water vapor (WV) and temperature (T) profiles with high accuracy and vertical resolution from the surface throughout the troposphere during daytime and nighttime are fundamental for accurate monitoring, weather forecasts, process studies, data assimilation, and validation of satellites. The mean profiles of T and WV, the statistics of their fluctuations, and flux profiles are also essential for energy and water budget studies. Therefore, these measurements are key for the understanding and the prediction of the diurnal cycle and the structure of the lower troposphere, in order to resolve the strength of the inversion layer at the planetary boundary layer (PBL) top, elevated lids in the free troposphere and turbulent fluctuations in WV and T, simultaneously during daytime and nighttime with a high temporal and range resolution. Consequently, high-performance WV and T profiling is fundamental for advanced weather and climate simulations.

Different techniques for measuring the atmospheric T profiles with lidar systems have been investigated in the last years, namely, the rotational Raman (RRL) technique, the integration technique (using elastic and Raman signals), the resonance fluorescence technique, and the high-spectral resolution lidar technique (see Behrendt, 2005, for an overview). For WV profiles, the Raman lidar technique and differential absorption lidar (DIAL) are available (Behrendt, 2005; Wulfmeyer et al., 2015).

Considering daytime measurements of T in the troposphere where always aerosol particles are present, the RRL technique is the most reliable lidar technique at date (Behrendt, 2005). It is straightforward to extend such a T lidar with a WV Raman channel to obtain combined measurements during nighttime and

daytime even within aerosol layers and thin clouds with high temporal and spatial resolution and low systematic and noise uncertainties (e.g., Behrendt et al., 2002; Di Girolamo et al., 2004; Hammann et al., 2015).

Passive remote sensing systems intrinsically lack the ability to resolve vertical structures in the order of a few hundred meter or less since their number of independent measurement points is limited (e.g., Wulfmeyer et al., 2016). Thus, several active remote sensing systems based on the lidar technology were developed in recent years to obtain operational or quasi-operational WV observations—and partly including also observations of T. In case of WV, the existing systems include the DIAL system of the National Center for Atmospheric Research (NCAR) (Spuler et al., 2015; Weckwerth et al., 2016), the the Raman lidar ofthe Jet Propulsion Laboratory (JPL) (Leblanc et al., 2012), and the Raman lidar of the Meteorological Research Institute (MRI) (Sakai et al., 2019). Both WV and T profiles are provided by the following lidar systems: the lidar of the Atmospheric Radiation Measurement (ARM) programSouthern Great Plains (SGP) site (Goldsmith et al., 1998; Newsom et al., 2013), RAMSES (Reichardt et al., 2012), and Raman LIDAR for Meteorological Observation (RALMO) lidar (Dinoev et al., 2013).

But none of these active remote sensing systems came close yet to fulfilling the WMO goal requirements for lower tropospheric profiling with respect to nowcasting and very short-range weather forecasting (see www.wmo-sat.info/oscar/observingrequirements), in the following abbreviated as "WMO VSRF goals." These requirements are more stringent than for high resolution numerical weather prediction (NWP).

While the SGP Raman Lidar was the only operational Raman Lidar so far which has been able to resolve turbulent WV fluctuations during daytime (Turner et al., 2014) only two nonautomatic systems have reported yet statistics of both turbulent WV and T fluctuations, namely, the University of Basilicata Raman lidar system (BASIL) (Paolo Di Girolamo et al., 2017) and the UHOH scanning Raman lidar (Hammann et al., 2015; Behrendt et al., 2015; Behrendt et al., 2019). But even these two systems were by far not yet advanced enough for coming close to the WMO VSRF goals—not even for single cases.

Satellite-based earth observation technology is not able to provide such data either. These systems have seen enormous progress in the last two decades. But despite these advances, substantial uncertainties in the interpretation of remotely sensed satellite data still exist (Stephens et al., 2012; Trenberth et al., 2009) and these observations are not capable to resolve the vertical structure of the PBL (Wulfmeyer et al., 2015).

Within the Modular Observation Solutions for Earth Systems project (https://www.ufz.de/moses/) of the Helmholtz Alliance, a new ground-based water-vapor and temperature remote sensing system fulfilling these requirements has been developed and tested by the Institute of Physics and Meteorology at the University of Hohenheim (UHOH). We call this new system ARTHUS (Atmospheric Raman Temperature and Humidity Sounder).

The aim of ARTHUS is to close this gap, which exist in satellite-based and ground-based Earth-observing systems, in order to provide reference data of these essential thermodynamic variables at day and night. It has already been shown that a strong positive impact on the skill of NWP models can be expected from less-advanced data (Adam et al., 2016; Dee et al., 2011; Wulfmeyer et al., 2015). We strived for turbulence resolution in WV and T profiling during daytime and nighttime, as this is key for the study of PBL process and land-atmosphere feedback (Wulfmeyer et al., 2018; Santanello et al., 2018) as well as for the development of turbulence parameterizations. ARTHUS is based on the knowledge acquired in the development of different generations of rotational Raman lidar systems in recent years (Behrendt et al., 2002, 2004; Behrendt & Reichardt, 2000; Hammann et al., 2015; Radlach, 2009).

This paper is structured as follows: The physical principles of Raman technique for WV and T measurements are summarized in section 2 demonstrating the potential of the optimization of daytime measurements. A description of ARTHUS follows in section 3, and the analysis of a measurement example in section 4. Section 5 shows comparisons between ARTHUS and radiosonde data. Finally, conclusions and an outlook are presented.

2. Raman Lidar Technique

Like any Raman lidar, also ARTHUS allows to measure the particle backscatter coefficient and the particle extinction coefficient independently (Ansmann et al., 1992; Weitkamp et al., 2009). Since such aerosol measurements are not new and not the focus here, we restrict the discussion to T and WV.

We obtain profiles of the WV mixing ratio $M(r)$ by dividing the WV Raman backscatter signal by the temperature-independent combination of the two rotational Raman signals (Behrendt et al., 2004) according to (e.g., Melfi et al., 1969; D. N. Whiteman et al., 1992, 2009; Whiteman, 2003)

$$M(\mathrm{r}) = C\frac{P_{WVRL}(r)}{P_{RRL1}(\mathrm{r}) + x\,P_{RRL2}(\mathrm{r})}\frac{\mathfrak{T}_{\nu_0}(\mathrm{r})}{\mathfrak{T}_{\nu_{WV}}(\mathrm{r})}$$

with $P_{WVRL}(r)$, $P_{RRL1}(r)$, and $P_{RRL2}(r)$ for the measured water vapor Raman signal and the two rotational Raman signals, respectively, C for the WV calibration, x for the combination factor to get a temperature-independent reference signal, and the last factor for the differential atmospheric transmission at the wavelength of the water vapor Raman signal and the rotational Raman signals, respectively.

The ratio Q of the high to low rotational quantum number Raman signals is used to obtain the atmospheric T profile (e.g., Behrendt, 2005). For temperature profiling, a calibration using three calibration constants *a, b, and c* is preferable (Behrendt, 2005) with

$$T(r) = \left(-\frac{b}{2a} - \sqrt{\left(\frac{b}{2a}\right)^2 - \frac{c - Log(Q)}{a}}\right)^{-1}$$

The calibration constants are determined by comparison with other sensors such as narrow-band WV DIAL, radio soundings, other in situ sensors, or a theoretical analysis of the receiver transmission functions. In a variety of publications, it was confirmed that these system constants of well-engineered Raman lidars are very stable so that a very good long-term stability and accuracy of the measured profiles is achieved (Turner et al., 2002).

A huge advantage of ARTHUS is that both T and WV profiles can be measured simultaneously with just one laser transmitter. T and WV data can be combined to get relative humidity measurements which are useful for aerosol (Wulfmeyer & Feingold, 2000) and convection initiation studies (A. Behrendt et al., 2011). Since the primary wavelength can be selected in a flexible way, powerful and reliable frequency-tripled Nd:YAG laser can be used.

3. Lidar Setup

A single receiver extracts the three Raman backscatter signals. In addition, it makes sense to add a fourth channel for the elastic backscatter signal in order to obtain signals from aerosol layers and clouds. Furthermore, by error propagation of the received photon-counting signal, not only WV and T profiles but also their uncertainties are determined in near real time (Behrendt et al., 2015; Wulfmeyer et al., 2016). The receiver with these four signals can be designed in such a way that the signal extraction is very efficient, the background suppression in high, while at the same time the suppression of the elastic backscatter signal in the Raman channels is high. The result is a compact, reliable, and robust active remote sensing system which fits into a cabinet with a size of 2.6 m × 1.4 m × 2.1 m (W × D × H). Furthermore, it is fully operational and runs 24/7.

Fundamental for an operational system is the laser transmitter. It must run without maintenance for a long time period. Here the laser source is an injection-seeded Nd:YAG laser (InnoLas Laser GmbH, Germany). The manufacturer states a typical lifetime of operation of several years before it may be necessary that the laser diode bars need maintenance. Long-term experience is now required in order to confirm this statement. The laser pulse energy in the UV is 100 mJ at a repetition rate of 200 Hz. The first and second harmonics are separated spatially from the third harmonic using a Pellin-Broca prism and blocked, so no other radiation than the third-harmonic radiation at 354.83 nm is transmitted into the atmosphere. This is quite beneficial for eye-safety considerations. Since this part of the UV permits comparatively high maximum exposure regarding eye safety (see the norms DIN EN 60 825-1, IEC 60825-1, and ANSI +Z136.1-2014 which all agree here), the maximum emitted energy density of 2 mJ/cm^2 in the peak of the ARTHUS beam profile, is not only eye safe for single pulses but also for exposure times of up to 1.5 s, when it leaves the housing. Due to the beam divergence of about 0.2 mrad, the allowed exposure times furthermore increase with range. Thus, any airborne platforms moving with at least a few centimeters per second are within eye safety

limits. Wherever this should not be considered as safe enough for all practical means, even longer eye safe exposure times could be accomplished by further beam expansion or an automatic beam shutter could be implemented which detects blocking of the beam.

The receiving telescope is a Ritchey-Chrétien-Cassegrain type. Its primary mirror has a diameter of 40 cm. The coating is optimized for the UV. A fiber guides the collected radiation backscattered from the atmosphere to a polychromator containing the four acquisition channels. Here improvements in the receiving chain include new interference filters with higher transmission for the elastic and Raman channels compared to previous versions (see Hammann et al., 2015).

The incoming light is directed to a dichroic beam splitter (Chroma), which splits it into two beams (Hammann et al., 2015). Wavelengths longer than 375 nm are reflected while shorter wavelengths are transmitted. The vibrational Raman signal of water vapor at 407.7 nm is obtained from the reflected beam. The transmission efficiency of the beam splitter is 0.95 between 350 and 375 nm and 0.02 for 408 nm. Reflectivity at 408 nm is above 0.95.

The signal transmitted by the beam splitter passes a daylight-reducing filter (Laser components, peak transmission of 0.92) and enters the main part of the receiver for the detection of the elastic and rotational Raman signals, which are sequentially mounted (Behrendt et al., 2002; Hammann et al., 2015; Radlach et al., 2008).

In front of the elastic channel and also each rotational Raman channel, there is an interference filter to achieve adequate suppression of the elastic signal, so leakage in the Raman channels is avoided. Overall transmission efficiency is 0.48, 0.34, 0.41, and 0.41 for the elastic, RR1, RR2, and WV channel, respectively. These filters allow for a strong reduction of the daylight background and avoid any leakage of the elastic signal in the Raman channels even in the presence of boundary layer clouds, which eliminates systematic errors and permits measurements into clouds up to an optical thickness of 3.

In all four channels, the extracted light is focused on photomultipliers (R9880U, Hammamatsu Photonics, Japan). The detected signals are then stored in analog and in photon-counting (PC) mode with 7.5-m resolution with a transient recorder (LICEL GmbH, Germany). During the measurements shown in this paper, backscatter signals of 2,000 shots, equal to a 10-s mean, were averaged. After dead-time correction of the PC data, the data is background-corrected.

The statistical uncertainty of the measurements is derived from the measured number of photon counts (or virtual photon counts in case of the analog signals) using error propagation (Behrendt et al., 2002; Wulfmeyer et al., 2016). This approach covers the so-called shot noise, which is the main error source in Raman lidar signals. The total statistical uncertainty can be obtained from an autocorrelation analysis of a time series of the fluctuations of a measured parameter (Behrendt et al., 2015; Lenschow et al., 2000; Wulfmeyer et al., 2016). This technique allows for separating noncorrelated noise from correlated atmospheric fluctuations, so profiles of the total noise uncertainty and profiles of higher-order moments of the atmospheric fluctuations (with their uncertainties) are obtained simultaneously. In the following, we apply this latter approach.

The four measured signals allow to derive four independent parameters: T, WV mixing ratio (MR), particle backscatter coefficient β, and particle extinction coefficient α (Behrendt et al., 2002). Higher level products are potential temperature, gradient of temperature and potential temperature, higher moments of turbulent T and WV fluctuations, relative humidity, buoyancy, convective available potential energy, and convective inhibition (Hammann et al., 2015).

4. Case Study and Performance

ARTHUS was operated for >2,500 hr between March 2018 and the submission of this paper in September 2019. Between 24 October 2018 and 14 November 2018 (22 days), the lidar was tested at the new site of the Land Atmosphere Feedback Observatory (LAFO; see lafo.uni-hohenheim.de (n.d.); Späth et al., 2019). The weather conditions correspond to fall time in Germany. It also participated in the ScaleX measurement campaign in southern Germany (14 May 2019 to 11 June 2019, 32 days), together with several other instruments (see https://scalex.imk-ifu.kit.edu). Since this period was in spring time in Germany, we faced fog, snow, clouds, and rain, given that the site was located at the top of a hill, about 1,000 m ASL. A third

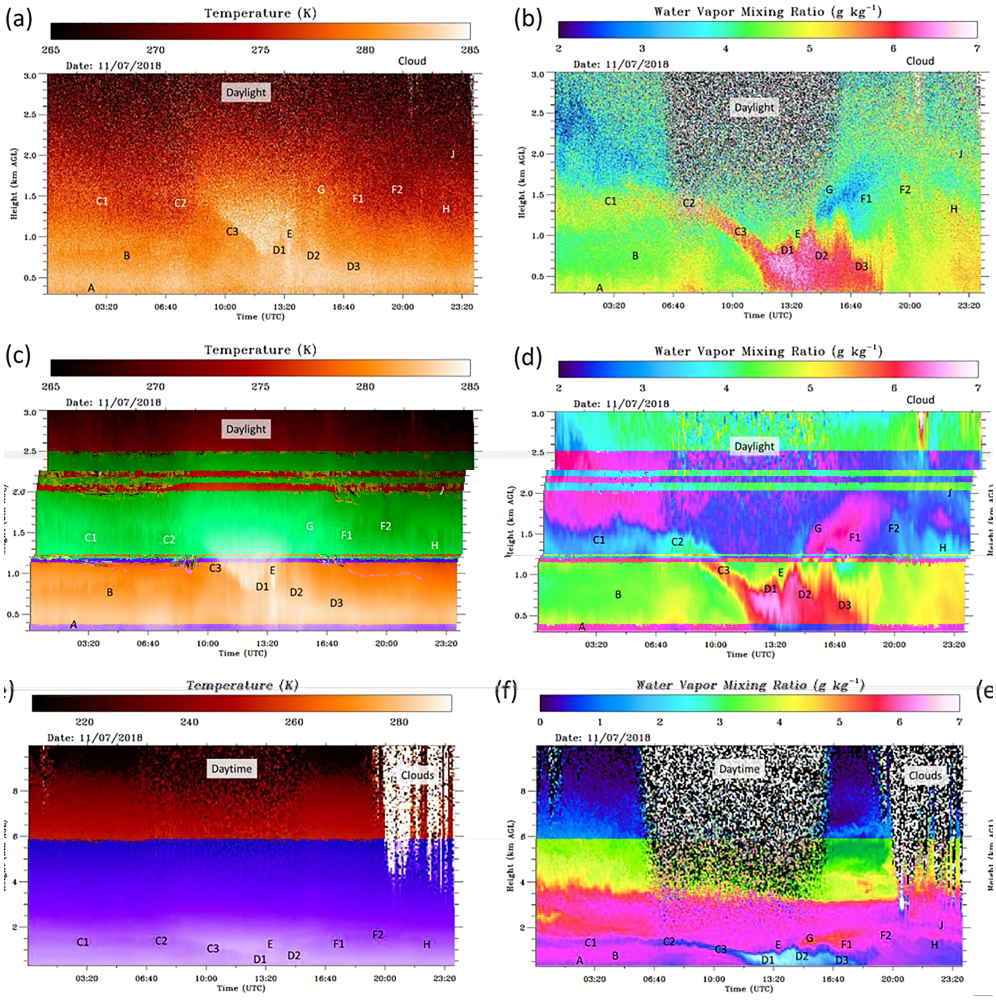

Figure 1. Time-height cross section of WV MR (right plots) and T (left plots) measured on 7 November 2018 between 00:00 and 24:00 UTC. Local noon was at 11:30 UTC. The resolution of the data in (a) and (b) is 7.5 m and 10 s while it is 300 s and a gliding average of 97.5 m in the other plots. Note the different scales for plots (e) and (f). Letters indicate several layers present on this day clearly visible by WV MR as well as temperature gradients, among these are, for example, an elevated humidity layer (C1 to C3) and the convective boundary layer (D1 to D3). AGL = Above ground level.

campaign took place at the German Weather Service (DWD) observatory site in Stuttgart Schnarrenberg, Germany, between 23 August 2019 and 25 September 2019 (33 days total) in the transition of summer to autumn time, some days with clouds, fog, and rain. Although we gathered a lot of interesting cases during these periods, we must restrict ourselves in this letter and can show only two of them, given the limited space allowed.

In the following, we focus on a case study for illustrating ARTHUS' performance during a test campaign at the LAFO site. Figure **1** shows an overview of the 24-hr data measured on 7 November 2018.

Analog and PC data were merged at 3 km. In order to calibrate the temperature and WV MR, radiosonde data of the closest radiosonde available, namely, of the DWD in Stuttgart, 13 km away were used. The development of the PBL can be seen in the both temperature and humidity data. Furthermore, differences in noise between day and night are seen in higher altitudes. With 5-min averaging and a gliding average of 97.5 m, the noise is reduced significantly compared to the raw data resolution. Four kilometers can be reached during daytime with the averaged WV data so that several layers as well as their changes in time can be made out. In the temperature case, differences in noise between day and night can hardly be seen up to 6 km in the averaged data and temperature gradients related to the layers can be observed. In the high-resolution measurements, even the convective eddies in the daytime PBL can be identified in both data sets as well as the

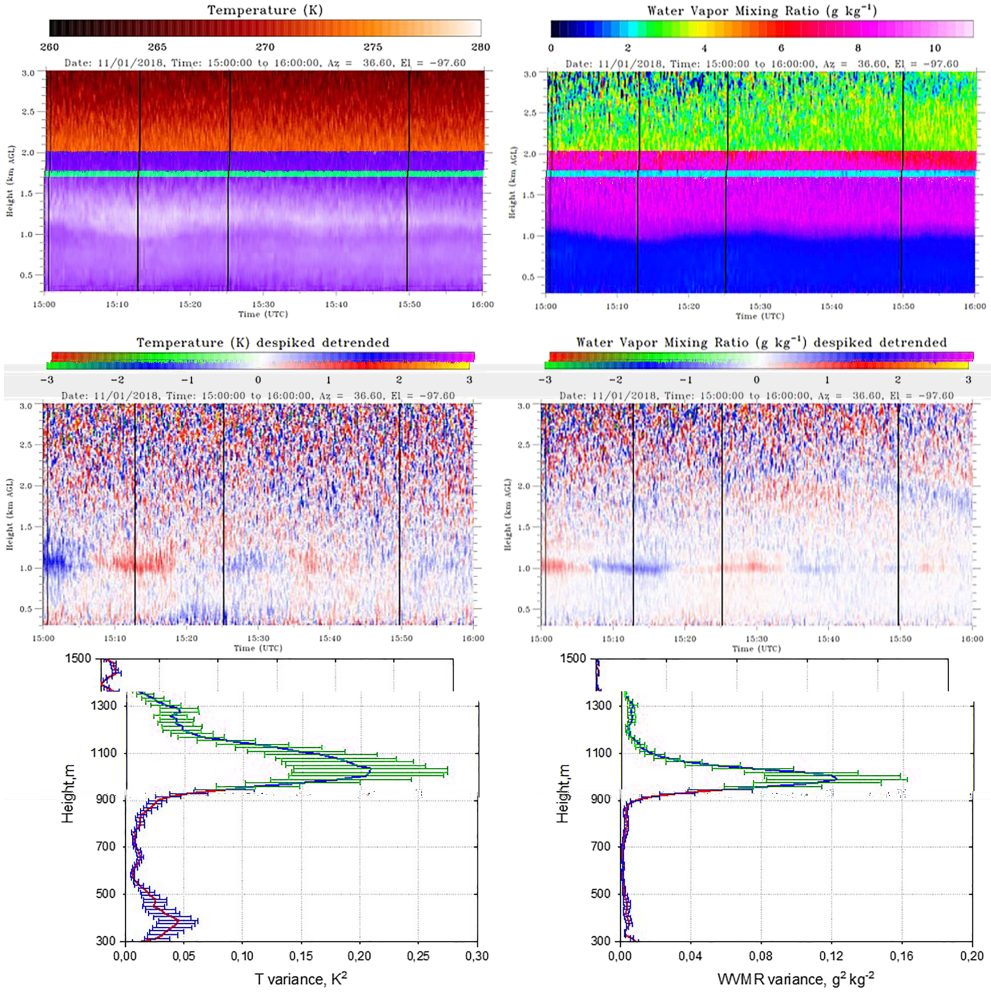

Figure 2. (top)T and WV measurements between 15:00 and 16:00 UTC on 1 November 2018 (resolution of 10 s and gliding average of 97.5 m). (middle) Despiked and detrended WV and T fluctuations. (bottom) Variance profiles of the atmospheric fluctuations.

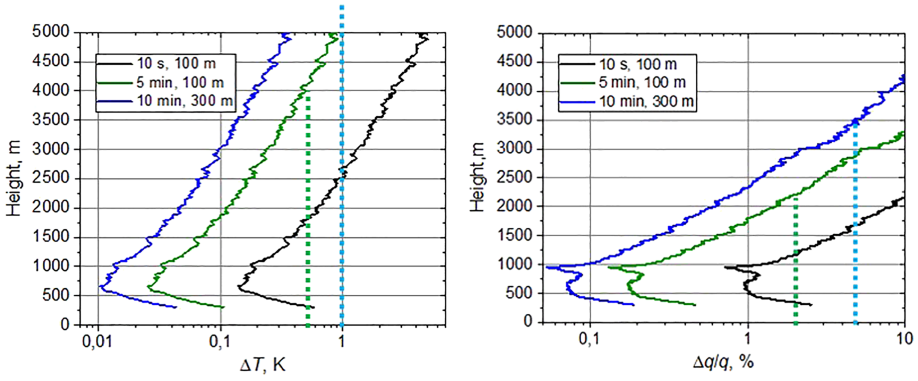

Figure 3. Total statistical uncertainties of the ARTHUS T and WV measurements for different temporal and spatial resolutions of the data. With increasing range, the uncertainties increase nearly exponentially above the overlap region. Dashed lines show the breakthrough requirements (blue, Δt = 10 min and Δz = 300 m) and goal requirements (green, 5 min and 100 m) of WMO for nowcasting and very short range weather forecasting in the lower troposphere. ARTHUS data fulfill these requirements in the PBL and lower free troposphere.

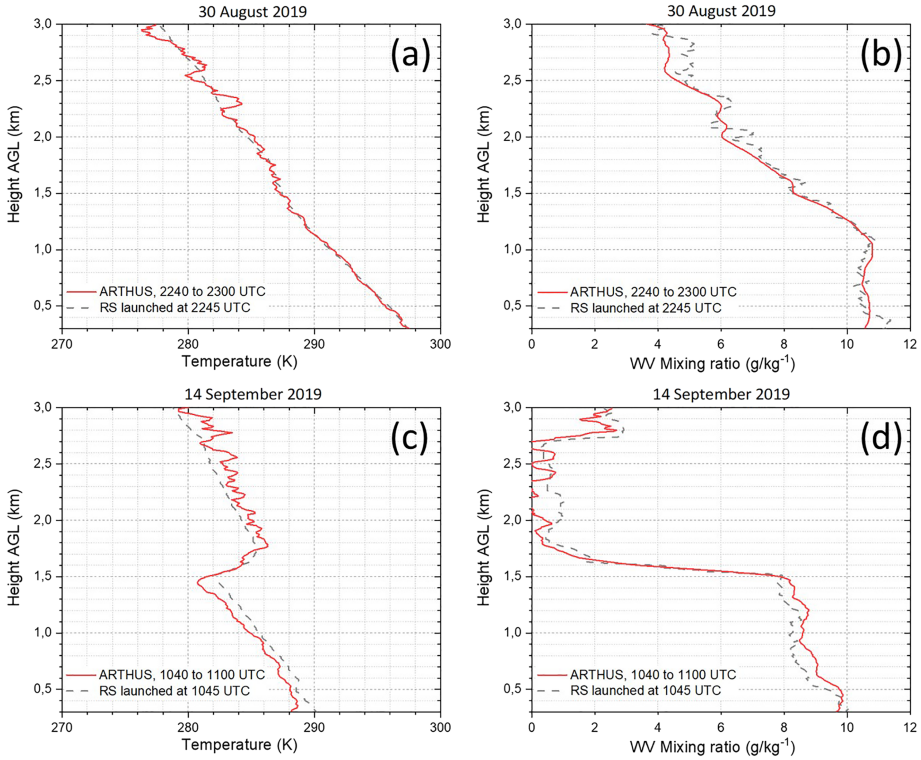

Figure 4. T and WV MR measurements of ARTHUS compared with data of radiosondes (Vaisala RS41) launched at the same site at the DWD observatory, Stuttgart Schnarrenberg. (a and b) Night measurements on 30 August 2019. For the ARTHUS profiles the data between 2240 and 2300 UTC were averaged. The radiosonde was launched at 2245 UTC. The measurements of ARTHUS were calibrated with these radiosonde data. (c and d) Noon measurements on 14 September 2019. ARTHUS data averaged from 1040 to 1100 UTC, radiosonde launched at 1045 UTC. Same calibrations as in (a) and (b).

gradients at the top of the PBL. It is important to note that the high resolutions of 10 s and 7.5 m have never been accomplished before. For the first time, we observed inversion layers in the free troposphere (Figure 1), which is not possible with any other ground-based remote sensing system.

In the following, a detailed error analysis is presented. We selected for this the period between 15 and 16 UTC on 7 November 2018 (Figure 2). During this time, a gravity wave was present which oscillated the PBL top in height. This caused the fluctuations of T and WV to vary in an anticorrelated way. While dry fluctuations were generally colder, moist ones were warmer. The same was found less pronounced in the PBL. The mean atmospheric variances, determined with the method of Lenschow et al. (2000) and Wulfmeyer et al. (2016), show peaks at the PBL top at about 1,000 m above ground level with maximum values of about 0.12 $(g/kg)^2$ and 0.2 K^2, respectively. It is very interesting to note that such small fluctuations can clearly be resolved with ARTHUS.

Together with the mean atmospheric variances, we obtained the statistical uncertainties (Figure 3). In a first step, we got the uncertainty profiles for the data resolution of 10 s and 97.5 m which we used for the analysis of the fluctuations (Figure 2). These profiles, can then be scaled to other temporal and spatial resolutions Δt and Δz, respectively, via

$$\sigma \propto (\Delta t\, \Delta z)^{-0.5}$$

with σ for the statistical uncertainty.

The WMO breakthrough requirements for nowcasting/VSRF for WV and T are reached up to 3.5 km and more than 5 km, respectively. Even the very stringent goal requirements of 2% and 0.5 K for a resolution of 5 min and 100 m is reached up to 2.2 and 4 km, respectively.

5. Observation Comparisons

ARTHUS was moved to the DWD site in Stuttgart in summer 2019. At ~50-m distance to ARTHUS, radiosondes were launched which gave the opportunity to intercompare the measurements with small sampling uncertainties. Examples of the data are shown in Figure 4.

The calibration of ARTHUS was made with nighttime data close to 0 UTC on 31 August 2019. As example for daytime measurements, we selected the data of 14 September 2019 (unchanged calibration of ARTHUS); interestingly, quite strong T and MR gradients were present at the top of the PBL at this day. The data of ARTHUS and the radiosonde are very close and the observed gradients are very similar despite of the different sampling methods and that the PBL was convective.

6. Conclusions

We demonstrated a breakthrough of the Raman lidar technique for daytime and nighttime WV and T profiling with high resolution and accuracy. A comprehensive analysis of the data confirms that the WMO goal requirements for VSRF can be met during daytime with ARTHUS. We showed that range-resolved measurements of WV MR were performed with a statistical uncertainty of less than 2% up to 2.2 km using a temporal resolution of 5 min and a vertical resolution of 100 m. Vertical measurements of temperature were performed with an uncertainty of less than 0.5 K and the same temporal and vertical resolutions up to more than 5 km. ARTHUS performance makes it possible to observe for the first time the strength of the inversion layer at the PBL top, elevated lids in the free troposphere during daytime and nighttime and the resolution of turbulent fluctuations in water vapor and temperature simultaneously also during daytime.

The nighttime performance, for example, for studying the nocturnal planetary boundary layer and tropospheric lidar, is even much better due the absence of daylight background. The interference filters allow a strong reduction of the daylight background and avoid leakage of the elastic signal in the Raman channels even in the presence of boundary layer clouds (or optically thin clouds) which eliminates systematic errors.

This confirms that ARTHUS is an exceptional tool for observations in the atmospheric boundary layer, since new science questions can be addressed such as improvement of weather forecast models by means of data assimilation, for instance, the detection of elevated layers is crucial for the prediction of convection initiation. Also, studies of turbulent transport in the convective boundary layer and studies of land-atmosphere feedback, which requires the resolution and characterization of turbulent transport of heat and matter.

The uncertainty analysis, however, did not yet include systematic errors. The results are nevertheless very promising. Further intercomparison campaigns are already planned for the near future. Given the thermal stability of the housing and that the laser is injection seeded, we expect that the systematic uncertainties are much smaller than the statistical ones.

Due to the relatively low power requirement (<5 kW depending mainly on the need for air conditioning) and the compact setup of ARTHUS, ground-based stations and networks can be set up or extended for climate monitoring, verification of weather, and climate and earth system models and data assimilation for improving weather forecasts, process studies as well as a calibration of and a synergy with passive remote sensing systems such as microwave radiometers and Fourier transform infrared spectrometers as well as radio soundings.

A very short latency of the delivery of data within minutes including all error profiles and the error covariance matrix is possible. This performance serves very well the next generation of very fast rapid-update-cycle data assimilation systems for nowcasting and short-range weather forecasting (Adam et al., 2016).

It is important to note that the assimilation of these thermodynamic profiles will also advance considerably the impact of radar data assimilation. Currently, the assimilation of radar data is strongly suffering from the missing knowledge of the thermodynamic environment around clouds and precipitation resulting in severe model in-balance problems. A new synergy of ARTHUS-like systems and radar networks would reduce these imbalances considerably increasing also the benefit of radar observations. Additionally, in the future, it will be possible to operate corresponding lidar systems also on shipborne and airborne platforms as well as in networks over land. Furthermore, spaceborne operation of WW and T Raman lidar has the potential to

provide global-scale WV MR and temperature measurements from the surface to the middle troposphere (Paolo Di Girolamo et al., 2018).

ARTHUS will be a part of the new infrastructure planned to complement the existing Helmholtz observatories, showing the potential of remote sensing systems gathering ground-truth information about land-atmosphere feedback, the behavior of the ABL and the lower troposphere. Also, due to its mobility and easy application in different regions of the earth and on different platforms, it will be available for various international field activities.

Acknowledgments
This work was funded by the Helmholtz Association of German Research Centers within the Modular Observation Solutions for Earth Systems project. We like to thank Shravan Kumar Muppa for his help with the error analysis, Timo Keller and Florian Späth for supporting the setup of the instrument at the campaign sites and our colleagues of DWD Schnarrenberg for their support. Data used in this paper is available at https://doi.pangaea.de/10.1594/PANGAEA.909871, following the AGU Data Policy.

References

Adam, S., Behrendt, A., Schwitalla, T., Hammann, E., & Wulfmeyer, V. (2016). First assimilation of temperature lidar data into an NWP model: Impact on the simulation of the temperature field, inversion strength and PBL depth. *Quarterly Journal of the Royal Meteorological Society*, *142*(700), 2882–2896. https://doi.org/10.1002/qj.2875

Ansmann, A., Wandinger, U., Riebesell, M., Weitkamp, C., & Michaelis, W. (1992). Independent measurement of extinction and backscatter profiles in cirrus clouds by using a combined Raman elastic-backscatter lidar. *Applied Optics*, *31*(33), 7113. https://doi.org/10.1364/AO.31.007113

Behrendt, A. (2005). Temperature measurements with lidar. In C. Weitkamp (Ed.), *Lidar* (pp. 273–305). New York, NY: Springer New York. https://doi.org/10.1007/0-387-25101-4_10

Behrendt, A., Pal, S., Aoshima, F., Bender, M., Blyth, A., Corsmeier, U., et al. (2011). Observation of convection initiation processes with a suite of state-of-the-art research instruments during COPS IOP 8b. *Quarterly Journal of the Royal Meteorological Society*, *137*(S1), 81–100. https://doi.org/10.1002/qj.758

Behrendt, A., Wulfmeyer, V., Senff, C., Muppa, S. K., Späth, F., Lange, D., et al. (2019). Observation of sensible and latent heat flux pofiles with lidar. *Atmos. Meas. Tech. Discuss*. https://doi.org/10.5194/amt-2019-305

Behrendt, A., Wulfmeyer, V., Hammann, E., Muppa, S. K., & Pal, S. (2015). Profiles of second- to fourth-order moments of turbulent temperature fluctuations in the convective boundary layer: First measurements with rotational Raman lidar. *Atmospheric Chemistry and Physics*, *15*(10), 5485–5500. https://doi.org/10.5194/acp-15-5485-2015

Behrendt, A., Nakamura, T., Onishi, M., Baumgart, R., & Tsuda, T. (2002). Combined Raman lidar for the measurement of atmospheric temperature, water vapor, particle extinction coefficient, and particle backscatter coefficient. *Applied Optics*, *41*(36), 7657–7666. https://doi.org/10.1364/AO.41.007657

Behrendt, A., Nakamura, T., & Tsuda, T. (2004). Combined temperature lidar for measurements in the troposphere, stratosphere, and mesosphere. *Applied Optics*, *43*(14), 2930–2939. https://doi.org/10.1364/ao.43.002930

Behrendt, A., & Reichardt, J. (2000). Atmospheric temperature profiling in the presence of clouds with a pure rotational Raman lidar by use of an interference-filter-based polychromator. *Applied Optics*, *39*(9), 1372–1378. https://doi.org/10.1364/ao.39.001372

Dee, D. P., Uppala, S. M., Simmons, A. J., Berrisford, P., Poli, P., Kobayashi, S., et al. (2011). The ERA-Interim reanalysis: Configuration and performance of the data assimilation system. *Quarterly Journal of the Royal Meteorological Society*, *137*(656), 553–597. https://doi.org/10.1002/qj.828

Di Girolamo, P., Behrendt, A., & Wulfmeyer, V. (2018). Space-borne profiling of atmospheric thermodynamic variables with Raman lidar: Performance simulations. *Optics Express*, *26*(7), 8125–8161. https://doi.org/10.1364/OE.26.008125

Di Girolamo, P., Marchese, R., Whiteman, D. N., & Demoz, B. B. (2004). Rotational Raman lidar measurements of atmospheric temperature in the UV. *Geophysical Research Letters*, *31*, L01106. https://doi.org/10.1029/2003GL018342

Dinoev, T., Simeonov, V., Arshinov, Y., Bobrovnikov, S., Ristori, P., Calpini, B., et al. (2013). Raman Lidar for Meteorological Observations, RALMO—Part 1: Instrument description. *Atmospheric Measurement Techniques*, *6*(5), 1329–1346. https://doi.org/10.5194/amt-6-1329-2013

Girolamo, P. D., Cacciani, M., Summa, D., Scoccione, A., Rosa, B. D., Behrendt, A., & Wulfmeyer, V. (2017). Characterisation of boundary layer turbulent processes by the Raman lidar BASIL in the frame of HD (CP)2 Observational Prototype Experiment. *Atmospheric Chemistry and Physics*, *17*(1), 745–767. https://doi.org/10.5194/acp-17-745-2017

Goldsmith, J. E. M., Blair, F. H., Bisson, S. E., & Turner, D. D. (1998). Turn-key Raman lidar for profiling atmospheric water vapor, clouds, and aerosols. *Applied Optics*, *37*(21), 4979–4990. https://doi.org/10.1364/AO.37.004979

Hammann, E., Behrendt, A., Le Mounier, F., & Wulfmeyer, V. (2015). Temperature profiling of the atmospheric boundary layer with rotational Raman lidar during the HD (CP)2 Observational Prototype Experiment. *Atmospheric Chemistry and Physics*, *15*(5), 2867–2881. https://doi.org/10.5194/acp-15-2867-2015

lafo.uni-hohenheim.de. (n.d.). Retrieved June 18, 2019, from https://lafo.uni-hohenheim.de/en/1670

Leblanc, T., McDermid, I. S., & Walsh, T. D. (2012). Ground-based water vapor raman lidar measurements up to the upper troposphere and lower stratosphere for long-term monitoring. *Atmospheric Measurement Techniques*, *5*(1), 17–36. https://doi.org/10.5194/amt-5-17-2012

Lenschow, D. H., Wulfmeyer, V., & Senff, C. (2000). Measuring second- through fourth-order moments in noisy data. *Journal of Atmospheric and Oceanic Technology*, *17*(10), 1330–1347. https://doi.org/10.1175/1520-0426(2000)017<1330:MSTFOM>2.0.CO;2

Melfi, S. H., Lawrence, J. D., & McCormick, M. P. (1969). Observation of raman scattering by water vapor in the atmosphere. *Applied Physics Letters*, *15*(9), 295–297. https://doi.org/10.1063/1.1653005

Newsom, R. K., Turner, D. D., Goldsmith, J. E. M., Newsom, R. K., Turner, D. D., & Goldsmith, J. E. M. (2013). Long-term evaluation of temperature profiles measured by an operational Raman lidar. *Journal of Atmospheric and Oceanic Technology*, *30*(8), 1616–1634. https://doi.org/10.1175/JTECH-D-12-00138.1

Radlach, M.. (2009). A scanning eye-safe rotational Raman lidar in the ultraviolet for measurements of tropospheric temperature fields. Universität Hohenheim.

Radlach, M., Behrendt, A., & Wulfmeyer, V. (2008). Scanning rotational Raman lidar at 355 nm for the measurement of tropospheric temperature fields. *Atmospheric Chemistry and Physics*, *8*(2), 159–169. https://doi.org/10.5194/acp-8-159-2008

Reichardt, J., Wandinger, U., Klein, V., Mattis, I., Hilber, B., & Begbie, R. (2012). RAMSES: German Meteorological Service autonomous Raman lidar for water vapor, temperature, aerosol, and cloud measurements. *Applied Optics*, *51*(34), 8111–8131. https://doi.org/10.1364/AO.51.008111

Sakai, T., Nagai, T., Izumi, T., Yoshida, S., & Shoji, Y. (2019). Automated compact mobile Raman lidar for water vapor measurement: Instrument description and validation by comparison with radiosonde, GNSS, and high-resolution objective analysis. *Atmospheric Measurement Techniques*, *12*(1), 313–326. https://doi.org/10.5194/amt-12-313-2019

Santanello, J. A. Jr, Dirmeyer, P. A., Ferguson, C. R., Findell, K. L., Tawfik, A. B., Berg, A., et al. (2018). Land-Atmosphere Interactions: The LoCo Perspective. *Bulletin of the American Meteorological Society*, *99*, 1253–1272. https://doi.org/10.1175/BAMS-D-17-0001.1

Späth, F., Veresteck, V., Wulfmeyer, V., Streck, T., & Behrendt, A. (2019). The Land-Atmosphere Feedback Observatory (LAFO): A novel sensor network to improve weather forecasting and climate models. In EGU General Assembly. Vienna.

Spuler, S. M., Repasky, K. S., Morley, B., Moen, D., Hayman, M., & Nehrir, A. R. (2015). Field-deployable diode-laser-based differential absorption lidar (DIAL) for profiling water vapor. *Atmospheric Measurement Techniques*, *8*(3), 1073–1087. https://doi.org/10.5194/amt-8-1073-2015

Stephens, G. L., Li, J., Wild, M., Clayson, C. A., Loeb, N., Kato, S., et al. (2012). An update on Earth's energy balance in light of the latest global observations. *Nature Geoscience*, *5*(10), 691–696. https://doi.org/10.1038/ngeo1580

Trenberth, K. E., Fasullo, J. T., Kiehl, J., Trenberth, K. E., Fasullo, J. T., & Kiehl, J. (2009). Earth's global energy budget. *Bulletin of the American Meteorological Society*, *90*(3), 311–324. https://doi.org/10.1175/2008BAMS2634.1

Turner, D. D., Ferrare, R. A., Brasseur, L. A. H., Feltz, W. F., & Tooman, T. P. (2002). Automated retrievals of water vapor and aerosol profiles from an operational Raman lidar. *Journal of Atmospheric and Oceanic Technology*, *19*(1), 37–50. https://doi.org/10.1175/1520-0426(2002)019<0037:AROWVA>2.0.CO;2

Turner, D. D., Wulfmeyer, V., Berg, L. K., & Schween, J. H. (2014). Water vapor turbulence profiles in stationary continental convective mixed layers. *Journal of Geophysical Research: Atmospheres*, *119*, 11,151–11,165. https://doi.org/10.1002/2014JD022202

Weckwerth, T. M., Weber, K. J., Turner, D. D., & Spuler, S. M. (2016). Validation of a water vapor micropulse differential absorption Lidar (DIAL). *Journal of Atmospheric and Oceanic Technology*, *33*(11), 2353–2372. https://doi.org/10.1175/JTECH-D-16-0119.1

Weitkamp, C., Wandinger, U., Michaelis, W., Riebesell, M., & Ansmann, A. (2009). Independent measurement of extinction and back-scatter profiles in cirrus clouds by using a combined Raman elastic-backscatter lidar. *Applied Optics*, *31*(33), 7113. https://doi.org/10.1364/ao.31.007113

Whiteman, D. N., Melfi, S. H., & Ferrare, R. A. (1992). Raman lidar system for the measurement of water vapor and aerosols in the Earth's atmosphere. *Applied Optics*, *31*(16), 3068–3082. https://doi.org/10.1364/AO.31.003068

Whiteman, D. N., Melfi, S. H., & Ferrare, R. A. (2009). Raman lidar system for the measurement of water vapor and aerosols in the Earth's atmosphere. *Applied Optics*, *31*(16), 3068. https://doi.org/10.1364/ao.31.003068

Whiteman, D. N. (2003). II. Evaluating the ratios for water vapor and aerosols. *Applied Optics*, *42*(15), 2593–2608. https://doi.org/10.1364/ao.42.002593

Wulfmeyer, V., & Feingold, G. (2000). On the relationship between relative humidity and particle backscattering coefficient in the marine boundary layer determined with differential absorption lidar. *Journal of Geophysical Research*, *105*(D4), 4729–4741. https://doi.org/10.1029/1999JD901030

Wulfmeyer, V., Hardesty, R. M., Turner, D. D., Behrendt, A., Cadeddu, M. P., Di Girolamo, P., et al. (2015). A review of the remote sensing of lower tropospheric thermodynamic profiles and its indispensable role for the understanding and the simulation of water and energy cycles. *Reviews of Geophysics*, *53*, 819–895. https://doi.org/10.1002/2014RG000476

Wulfmeyer, V., Muppa, S. K., Behrendt, A., Hammann, E., Späth, F., Sorbjan, Z., et al. (2016). Determination of convective boundary layer entrainment fluxes, dissipation rates, and the molecular destruction of variances: Theoretical description and a strategy for its confirmation with a novel Lidar system synergy. *Journal of the Atmospheric Sciences*, *73*(2), 667–692. https://doi.org/10.1175/JAS-D-14-0392.1

Wulfmeyer, V., Turner, D. D., Baker, B., Banta, R., Behrendt, A., Bonin, T., et al. (2018). A New Research Approach for Observing and Characterizing Land-Atmosphere Feedback. *Bulletin of the American Meteorological Society*, *99*, 1639–1667. https://doi.org/10.1175/BAMS-D-17-0009.1